Observations of internal wave packets propagating along-shelf in northern Monterey Bay

C. B. Woodson,[1] J. A. Barth,[2] O. M. Cheriton,[3] M. A. McManus,[4] J. P. Ryan,[5] L. Washburn,[6] Kristin N. Carden,[7] Brian S. Cheng,[8] Lauren E. Garske,[8] Tarik C. Gouhier,[9] Alison J. Haupt,[10] Kristen T. Honey,[10] Maxwell F. Hubbard,[11] Alison Iles,[9] Margaret C. Lynch,[7] Brenna Mahoney,[12] Malin L. Pinksy,[10] Matt J. Robart,[8] Julia S. Stewart,[10] Sarah J. Teck,[7] and Aaron True[13]

Received 10 September 2010; revised 25 October 2010; accepted 2 November 2010; published XX Month 2010.

[1] Internal waves of depression were observed propagating along-shelf and into northern Monterey Bay, California (CA) on the inner shelf. These waves had amplitudes approximately equal to the thermocline depth (~4 m), and were unstable to shear and mix the thermocline. Isopycnal gradient spectra showed that the wave packets lead to an elevated mean dissipation rate of $\varepsilon = 2.63 \times 10^{-5}$ m^3 s^{-2} for up to 2 hours after wave passage. The proximity to the surface created strong surface convergences that can actively transport buoyant material, such as plankton, back into the bay. The wave packets were observed regularly over the upwelling season across multiple years suggesting they may have large effects on the documented spatial variation of phytoplankton and larvae on the inner shelf. The timing of the waves suggests they are not formed by tides interacting with bathymetry, but are generated by buoyant plume propagation.

Citation: Woodson, C. B., et al. (2010), Observations of internal wave packets propagating along-shelf in northern Monterey Bay, *Geophys. Res. Lett.*, *37*, LXXXXX, doi:10.1029/2010GL045453.

1. Introduction

[2] Internal waves are important features in the coastal ocean due to their influence on density structure, energy transfer, and their significant effects on marine ecosystems [*Carter et al.*, 2005; *D'Asaro et al.*, 2007; *Moum et al.*, 2007; *Pineda et al.*, 2007; *Scotti and Pineda*, 2004]. Nonlinear internal waves are often observed as depressions or elevations of the pycnocline, and can appear as propagating slicks and rough patches on the ocean surface that are visible in synthetic aperture radar [SAR] images [*Fu and Holt*, 1982; *Trask and Briscoe*, 1983]. Such internal waves travel across the shelf after their generation near shelf breaks due to barotropic tidal interactions with bathymetry [*D'Asaro et al.*, 2007; *Jeans and Sherwin*, 2001a, 2001b; *Klymak and Moum*, 2003; *Kunze et al.*, 2002; *Moum et al.*, 2007]. Mixing and transport due to internal waves as they travel into the coastal zone are important to many coastal ocean processes [*Grimshaw et al.*, 1999; *Klymak and Moum*, 2003]. However, other mechanisms also lead to internal wave generation such as buoyant plume propagation [*Nash and Moum*, 2005; *Stashchuk and Vlasenko*, 2009; *Xing and Davies*, 2005] which can also affect coastal ecosystems through the enhancement of nutrients in the surface layer and the organization and transport of red-tide forming algae [*Ryan et al.*, 2008]. Many of these processes can occur within a few kilometers of the coast and are not accounted for in many energy budgets.

[3] During upwelling conditions, a convergent front forms inshore of the Point Año Nuevo upwelling jet, and propagates along-shelf as a supercritical buoyancy current modulated by along-shelf winds [*Woodson et al.*, 2009]. Here we present observations of an amplitude-ordered internal wave packet traveling within these warm waters and along-shelf over the northern Monterey Bay shelf. We use density and current measurements to estimate wave amplitude, stability, energy, and mixing. We use a novel technique to estimate turbulent dissipation rates, and hypothesize that during deceleration of the front due to diurnal winds, amplitude-ordered internal wave packets of depression propagate back into the Bay. We then discuss the frequency and orientation of observed internal wave packets to address the hypothesized generation mechanisms.

2. Data and Methods

[4] Internal wave activity on the northern Monterey Bay inner shelf was observed using 3 moorings deployed from 26 June–5 July 2008 offshore of Long Marine Laboratory,

[1]Environmental Fluid Mechanics Laboratory, Stanford University, Stanford, California, USA.
[2]College of Oceanic and Atmospheric Science, Oregon State University, Corvallis, Oregon, USA.
[3]Ecology and Evolutionary Biology, University of California, Santa Cruz, California, USA.
[4]Department of Oceanography, University of Hawai'i at Mānoa, Honolulu, Hawaii, USA.
[5]Monterey Bay Aquarium Research Institute, Moss Landing, California, USA.
[6]Geography Department, University of California, Santa Barbara, California, USA.
[7]Department of Ecology, Evolution, and Marine Biology, University of California, Santa Barbara, California, USA.
[8]Bodega Marine Laboratory, University of California, Davis, Bodega Bay, California, USA.
[9]Department of Zoology, Oregon State University, Corvallis, Oregon, USA.
[10]Hopkins Marine Station, Stanford University, Pacific Grove, California, USA.
[11]CODAR Ocean Sensors Ltd., Mountain View, California, USA.
[12]Department of Ecology, Evolution, and Marine Biology, University of California, Santa Cruz, California, USA.
[13]Civil and Environmental Engineering, Georgia Institute of Technology, Atlanta, Georgia, USA.

0094-8276/10/2010GL045453

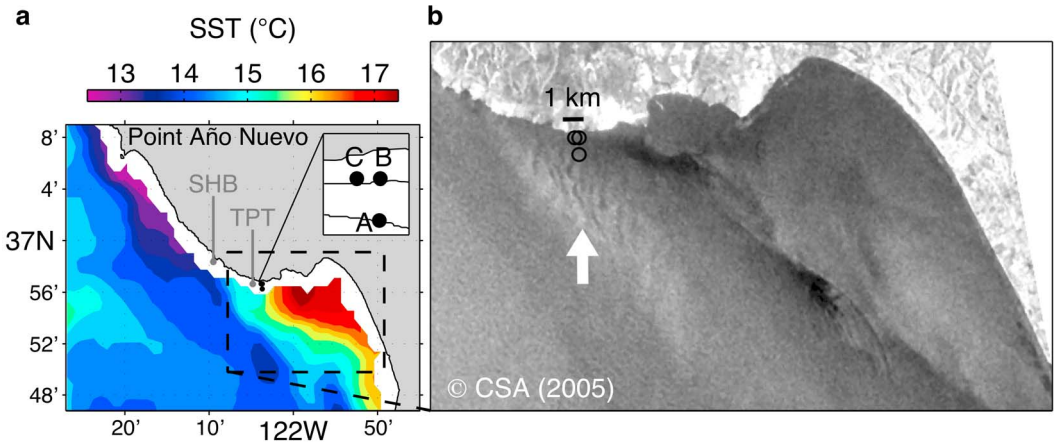

Figure 1. (a) Synoptic AVHHR SST image from 11 July 2005, 22:44:00 GMT and locations of moorings used in 2008 internal wave study. Inset shows moorings relative to 15-m and 25-m isobaths. (b) Synoptic SAR image from 11-Jul-2005, 02:03:02 GMT showing internal waves oriented perpendicular to shore and bounded by upwelling shadow in northern Monterey Bay.

Santa Cruz, CA as part of the 2008 Coastal Physical Oceanography and Marine Ecosystems course taught by the Partnership for the Interdisciplinary Study of the Coastal Ocean (PISCO) (Figure 1). The moorings were arranged in a right triangle with two moorings 250 m apart on the 15-m isobath (C, B), and a third mooring (A) approximately 500 m directly offshore from mooring B on the 25-m isobath. Typical thermocline depths within the upwelling shadow, a region of reduced wind in northern Monterey Bay, are 4–8 m depth [*Woodson et al.*, 2009]. Each mooring was equipped with SBE39 temperature loggers at 4, 6, and 8-m depth and at 1 m above bottom (mab; i.e. 14 or 24 m). SBE 39 thermistors sampled at 3-s sampling interval for up to 9 days. Surface temperatures were monitored using StowAway TidBit temperature loggers (Onset Computer Corp.) with a 2-min sampling interval. The sampling frequency and mooring spatial design allowed us to calculate propagation speeds and direction of internal wave packets as they passed through study site with error of less than 1% (estimated using mooring spacing and sampling rates). Salinity variation in northern Monterey Bay during the summer upwelling season is sufficiently small such that density is controlled by temperature as confirmed by shipboard conductivity-temperature-depth (CTD) profiles from a small research vessel during the 2008 deployment [*Woodson et al.*, 2009]. Therefore, we estimated density from temperature, assuming a mean observed salinity of 33.84; the maximum error using this approach is about 0.01 kg m^{-3}. We used isotherm following to estimate vertical velocities and turbulence associated with the internal wave packets. Isotherm displacement, ζ, was estimated using mean CTD profiles conducted within a few hours of wave arrival as $\zeta = z - Z_o(T)$ where z is the thermistor depth, $Z_o(T)$ is the depth at which the reference temperature profile is equal to the observed temperature, T [*Klymak and Moum*, 2007b]. Time was converted to a spatial domain using a Taylor-advection scheme as $x = (c - u)t$ where $(c - u)$ is the observed propagation speed (c) in the presence of a barotropic current (u). Spectra are then computed from the isopycnal gradient or slope, $d\zeta/dx$. Overall changes in the mean thermocline structure not resolved by the coarse thermistor array and over the relatively short time period do not affect the shape of the spectra within the internal wave and turbulence subranges ($10^{-2} < k_x < 10^{0}$ cpm).

[5] Eight wave packets were observed during our one-week sampling period always in the evening. In order to determine how representative these results were over longer time scales, we examined a multiple-year time series from long-term moorings maintained by the PISCO program (SHB and TPT, Figure 1a) and 10 years of SAR images (Figure 1b). Each long-term mooring consisted of a 600-kHz ADCP recording in mode 1 (45 ping ensembles, every 2 min) and temperature loggers (2 min sampling interval; StowAway Tidbits and XTIs, Onset Computer Corp.) at the surface, 5-m, 10-m, and 19-m depth (1 mab). The sampling intervals for the long-term moorings allowed identification of internal wave signatures, but did not provide sufficient temporal resolution to identify internal wave packet characteristics.

3. Wave Characteristics and Theoretical Comparisons

[6] In this contribution, we focus on the leading wave in a single packet of waves of depression that occurred in the late afternoon of 29 June 2008 (Figures 2a and 2b). Wave characteristics were estimated by numerical solution of the Dubreil-Jacotin-Long (DJL) equation in the presence of a mean barotropic current [*Lamb*, 2003]. The density structure preceding the wave approximated a two-layer system (Figure 2a, CTD profiles) so wave characteristics were also derived based on the two-layer wave theory detailed by *Bogucki and Garrett* [1993, hereafter BG93]. Based on previous observations in the area [e.g., *Woodson et al.*, 2009], the upper layer contained warm water from the upwelling shadow, a warm-water lens that develops in northern Monterey Bay during active upwelling [*Graham and Largier*, 1997], and the lower layer was cool, upwelled water that originated ~20 km to the northwest (Point Año Nuevo; Figure 1a) [*Rosenfeld et al.*, 1994]. The amplitude of the leading wave (a = 4.1 m) was of the same

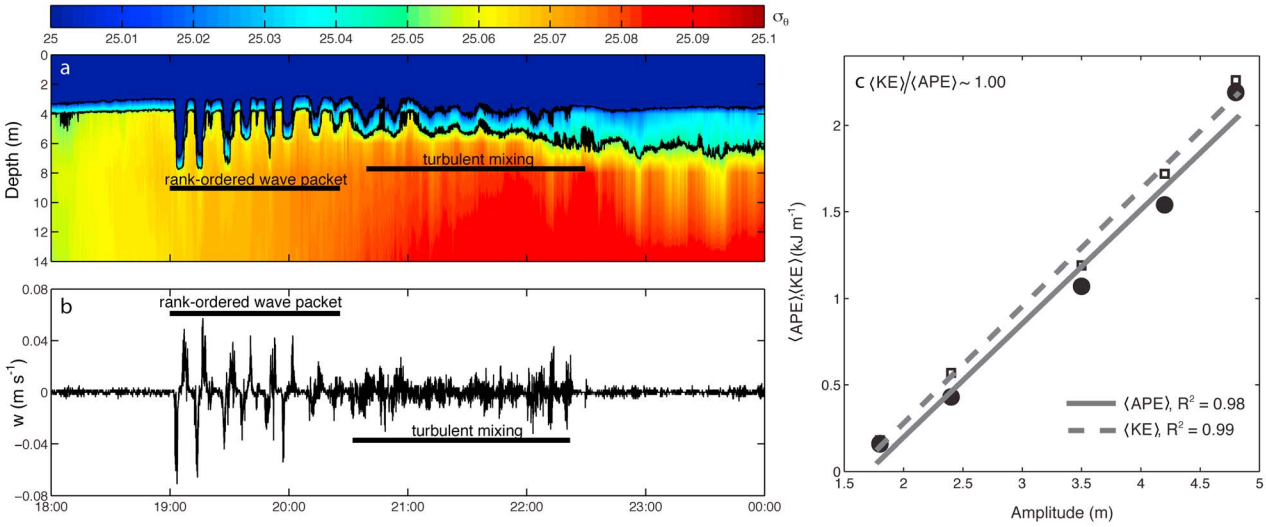

Figure 2. (a) Density contour plot from Mooring B (15-m water depth) showing internal wave packet. Black line and dots outline the 25 and 25.05 σ_θ isopycnals (a rough estimate of the pycnocline based on gradient strength). Width of thermocline grows from ~2 m to ~5 m after passage of wave packet. (b) Associated vertical velocities (w) calculated from isopycnal displacements, and (c) $\langle APE \rangle$ and $\langle KE \rangle$ versus internal wave amplitude for single rank-ordered wave packet estimated from the solutions of the DJL equation.

order as the upper layer depth (H = 3.8 m). Assuming a characteristic wave profile where displacement is $\eta(x, t) = a \sec h^2[(x - ct)/L]$, non-linear wave theory in a two-layer system described by BG93 suggests c = 0.12 m s^{-1} and a half-width, L: 28 m. The propagation speed and direction of travel were estimated from the mooring arrival times of the crest of the wave [*Lee*, 1961] and compared to theoretical values. Accounting for ambient currents (adding or subtracting observed barotropic currents from estimated propagation speeds) yields c = 0.11 m s^{-1} at bearing of 63°, which is into the Bay. The leading wave has an amplitude, a = 4.1 m, and L = 28 m. The width of the depression of the waves was estimated to be ~200 m. These lengths are the similar to those observed in SAR data sets with spatial structure of 200–1000 m (Figure 1).

4. Energy, Stability, and Transport

[7] Wave energy was computed by averaging and integrating the solution of the D-J-L equation over the wavelength of each wave [*Lamb*, 2003]. The energy contained in the wave packet was linearly correlated with amplitude (Figure 2c). The total energy density was approximately 12 kJ m^{-1} with the ratio of kinetic energy to available potential energy, $\langle KE \rangle / \langle APE \rangle$ ~ 1 across all waves, where $\langle\ \rangle$ indicates the spatial average across the wave. Energy flux across the wave group, computed as $\langle f_E \rangle = (c - u)\langle E \rangle$ to account for the effects of background currents, was 0.3 kW m^{-1}. The regularity of the waves over the upwelling season −68% of the total days in the season (~7 of 12 months of persistent upwelling favorable winds) as determined by SAR imagery and long-term moorings – and the width of the upwelling shadow (~3.5 km [*Woodson et al.*, 2009]) suggest a total energy transport of up to 150 MW-days per year into the bay.

[8] Barad and Fringer [*Barad and Fringer*, 2010] provided a correction to the shear stability analysis of BG93 due to observations of critical Richardson numbers of 0.1 instead of 0.25 as assumed. Incorporating this correction into estimates of the critical wave height required for shear instability yields a/H = 0.968 where H is the upper layer depth (3.8 m in this study). This suggests that the leading wave, with a/H = 1.08, is susceptible to shear instability. The trailing wake of the wave packet, with a thickened thermocline, and associated turbulent-like fluctuations of the isopycnals indicated the observed waves actively mixed the water column (Figure 2b). Solutions to the D-J-L equations also yielded Richardson numbers below the revised critical value of 0.1.

[9] The proximity of the thermocline to the surface leads to alternating strong surface convergences and divergences that move with the leading edge of the waves at speed, $u_{obs} = c - u$ = 0.03 m s^{-1}. Buoyant material, such as plankton, that is aggregated in the surface convergence consequently experience a weak net eastward transport against the mean barotropic flow which is westward and out of the Bay at ~0.1 m s^{-1} since $c > u$ [*Woodson et al.*, 2009]. The transport and structuring of plankton distributions will likely be strongly affected by the alternating convergence-divergence patterns in these frequently-occurring wave packets [*Ryan et al.*, 2005].

5. Turbulence and Mixing

[10] Turbulent dissipation was estimated using isopycnal slope spectra over both the internal wave and turbulence subranges ($10^{-2} < k_x < 10^0$ cpm) [*Klymak and Moum*, 2007a, 2007b]. The dissipation rate associated with the turbulent wake of the waves was derived from the spreading of the thermocline and the observed stratification as $K_\rho = F/(\partial\rho/\partial z)$ and $\varepsilon = K_\rho N^2/\Gamma$ [*Klymak and Moum*, 2007a, 2007b], where F; $\Delta\rho(\Delta h/\Delta t)$ is defined as the vertical density flux per unit length computed as the change in the center of mass of the water column (Δh) divided by the time

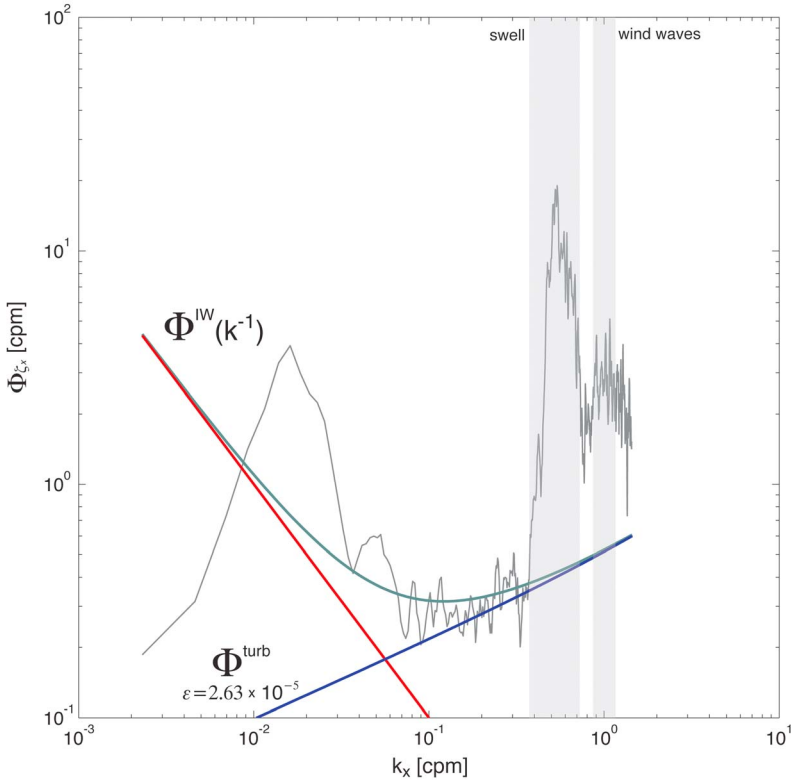

Figure 3. Isopycnal slope spectra (black line) for 6-hr period centered on internal wave observation on 27 June 2008. $\Phi_{\zeta_x}^{IW}$ (red line), $\Phi_{\zeta_x}^{Turb}$ (blue line), and linear combination (green line) fits are computed as described in text.

of active turbulent mixing. Δt is the time between last wave passage and end of observed thermocline thickening. The mixing efficiency, Γ, is assumed to be 0.2. This computation yielded a mean turbulent dissipation rate of $\varepsilon = 2.63 \times 10^{-5}\ m^3 s^{-2}$ for ~2 hr following wave passage.

[11] The isopycnal slope spectrum was smoothed using a 6-point geometric mean filter (thin black line, Figure 3). The internal wave subrange spectral component is estimated from theory as $\Phi_{\zeta_x}^{IW} = ak^p$ with a is a constant, and $p = -1$ (red line, Figure 3) and corresponds to a saturated subrange confined by the internal wave period (~10 min). The turbulence subrange consisting of both the inertial-convective and inertial-diffusive spectral components is computed as:

$$\Phi_{\zeta_x}^{Turb} = 4\pi\Gamma\varepsilon/N^2\left[C_T\varepsilon^{-1/3}(2\pi k_x)^{1/3} + q\nu^{1/2}\varepsilon^{-1/2}(2\pi k_x)\right]$$

where $C_T \approx 0.44$ and $q \approx 2.3$ are constants, and ν is the viscosity [*Klymak and Moum*, 2007a, 2007b]. Substituting in the estimated turbulent dissipation rate, ε, calculated from isopycnal spreading above yields the blue curve in Figure 3. The observed isopycnal slope spectrum fits theoretical spectrum, the sum of internal wave and turbulence components, reasonably well for $0.04 < k_x < 0.3$ cpm (green line, Figure 3; $R^2 = 0.78$). Deviation from the theoretical form at high wave numbers ($0.4 < k_x < 1$ cpm) results from swell and wind wave contamination. Deviation at low wave numbers ($k_x < 0.04$ cpm) may result from weak temperature fronts associated with larger-scale water masses. Surface wave contamination is also a significant issue when attempting to estimate Reynolds stresses and turbulent production from Acoustic Doppler Current Profilers (ADCPs) [*Rosman et al.*, 2008]. For isopycnal gradients, contamination of the spectra by surface waves ($0.4 < k_x < 1$ cpm) does not appear to significantly affect the fit at lower frequencies within the inertial-convective subrange allowing reasonable estimation of dissipation rates from these spectra in surface wave dominated coastal waters (Figure 3). The applicability of this technique to a wider range of conditions will however require further attention.

6. Potential Generation Mechanisms

[12] Internal wave generation in Monterey Bay frequently has been attributed to interactions of the internal tide with the Monterey Canyon [*Carter et al.*, 2005; *Kunze et al.*, 2002]. However, several factors suggest the waves observed here are not generated by internal tide propagation. First, upwelling jet waters originating near Point Año Nuevo are minimally stratified with strong overturning [*Rosenfeld et al.*, 1994], a dynamic situation that does not provide a propagation pathway onto the inner shelf. Second, these non-linear internal wave (NLIW) signals are not seen in SAR imagery north and outside of the upwelling shadow front (Figure 1b) or from moorings outside of the buoyant upwelling shadow. Third, the NLIWs were consistently observed during the late evening (2000–2300 local time) in both SAR imagery and moored observations. Finally, a 10-year record of SAR imagery indicates that internal waves along the northwest front boundary of the upwelling shadow occur more frequently during periods of strong diurnal wind forcing.

[13] Internal wave packets have been observed during the transition from supercritical ($Fr > 1$) to sub-critical ($Fr < 1$) flow for a surface front [*Nash and Moum*, 2005], and from modeling studies of bottom-associated tidal fronts [*Davies and Xing*, 2005; *Xing and Davies*, 2005]. Such waves could also be created through flow resonance [*Grimshaw and Smyth*, 1986; *Stashchuk and Vlasenko*, 2009]. Nonlinear, amplitude-ordered internal waves can be generated at $Fr > 1$, and can propagate downstream of a front [*Grimshaw and Smyth*, 1986].

[14] The lack of any significant topographic feature in the study area suggests that wave generation may be driven by variation in the flow field itself. In this case, local diurnal winds and buoyant plume propagation are the dominant mechanisms of flow variation [*Woodson et al.*, 2009]. Modulation of the front by diurnal wind forcing may thus lead to internal wave generation. The absence of other forcing mechanisms, the presence of the waves only within the buoyant upwelling shadow, and the orientation of the waves perpendicular to the coast support this mechanism for internal wave generation.

7. Summary and Conclusions

[15] Amplitude-ordered internal wave packets were observed traveling along-shelf and oriented perpendicular to shore along the northern edge of the Monterey Bay. These waves have a trailing turbulent field that mixes and thickens the pycnocline. The dissipation rate and mixing within the trailing wake of the wave packet was characterized using a novel application of the isotherm displacement technique first described for towed instruments [*Klymak and Moum*, 2007a, 2007b]. The transfer of energy away from the propagating front may be an important mechanism for preserving the front although interfacial stresses and wind forcing are also likely to be important [*Thomas and Ferrari*, 2008; *Woodson et al.*, 2009]. Similar 2-layer water masses forced by diurnal winds, such as occurs in the upwelling shadow in Monterey Bay, are prevalent features in this and other eastern boundary currents (e.g., the Peru-Chile Current System, the Benguela system, etc.) suggesting that internal wave generation by local winds and buoyant plume dynamics may be common in coastal upwelling systems.

[16] **Acknowledgments.** This is contribution 378 from PISCO, the Partnership for Interdisciplinary Studies of the Coastal Ocean, funded primarily by the Gordon and Betty Moore Foundation and the David and Lucile Packard Foundation. The authors would like to express gratitude to J. Nash and O. Fringer for discussion and review of earlier drafts, K. Lamb for providing *soliw* code, and the R/V Shana Rae (J. Christmann). The SAR image in Figure 1 was provided by the Canadian Space Agency, through the Alaska Satellite Facility.

References

Barad, M. F., and O. B. Fringer (2010), Simulations of shear instabilities in interfacial gravity waves, *J. Fluid Mech.*, *644*, 61–95, doi:10.1017/S0022112009992035.

Bogucki, D., and C. Garrett (1993), A simple model for the shear-induced decay of an internal solitary wave, *J. Phys. Oceanogr.*, *23*, 1767–1776, doi:10.1175/1520-0485(1993)023<1767:ASMFTS>2.0.CO;2.

Carter, G. S., et al. (2005), Internal waves, solitary-like waves, and mixing on the Monterey Bay shelf, *Cont. Shelf Res.*, *25*, 1499–1520, doi:10.1016/j.csr.2005.04.011.

D'Asaro, E. A., et al. (2007), High-frequency internal waves on the oregon continental shelf, *J. Phys. Oceanogr.*, *37*, 1956–1967, doi:10.1175/JPO3096.1.

Davies, A. M., and J. Xing (2005), The effect of a bottom shelf front upon the generation and propagation of near-inertial internal waves in the coastal ocean, *J. Phys. Oceanogr.*, *35*, 976–990, doi:10.1175/JPO2732.1.

Fu, L. L., and B. Holt (1982), Seasat views oceans and sea ice with synthetic aperture radar, *JPL Publ.*, *81–120*.

Graham, W. M., and J. L. Largier (1997), Upwelling shadows as nearshore retention sites: The example of northern Monterey Bay, *Cont. Shelf Res.*, *17*, 509–532, doi:10.1016/S0278-4343(96)00045-3.

Grimshaw, R., and N. Smyth (1986), Resonant flow of a statified fluid over topography, *J. Fluid Mech.*, *169*, 429–464, doi:10.1017/S002211208600071X.

Grimshaw, R., et al. (1999), Solitary wave transformation in a medium with sign-variable quadratic nonlinearity and cubic nonlinearity, *Physica D*, *132*, 40–62, doi:10.1016/S0167-2789(99)00045-7.

Jeans, D. R. G., and T. J. Sherwin (2001a), The evolution and energetics of large amplitude nonlinear internal waves on the Portuguese shelf, *J. Mar. Res.*, *59*, 327–353, doi:10.1357/002224001762842235.

Jeans, D. R. G., and T. J. Sherwin (2001b), The variability of strongly nonlinear solitary internal waves observed during an upwelling season on the Portuguese shelf, *Cont. Shelf Res.*, *21*, 1855–1878, doi:10.1016/S0278-4343(01)00026-7.

Klymak, J. M., and J. N. Moum (2003), Internal solitary waves of elevation advancing on a shoaling shelf, *Geophys. Res. Lett.*, *30*(20), 2045, doi:10.1029/2003GL017706.

Klymak, J. M., and J. N. Moum (2007a), Oceanic isopycnal slope spectra. Part II: Turbulence, *J. Phys. Oceanogr.*, *37*, 1232–1245, doi:10.1175/JPO3074.1.

Klymak, J. M., and J. N. Moum (2007b), Oceanic isopycnal slope spectra. Part I: Internal waves, *J. Phys. Oceanogr.*, *37*, 1215–1231, doi:10.1175/JPO3073.1.

Kunze, E., et al. (2002), Internal waves in Monterey Submarine Canyon, *J. Phys. Oceanogr.*, *32*, 1890–1913, doi:10.1175/1520-0485(2002)032<1890:IWIMSC>2.0.CO;2.

Lamb, K. G. (2003), Shoaling solitary internal waves: On a criterion for the formation of waves with trapped cores, *J. Fluid Mech.*, *478*, 81–100, doi:10.1017/S0022112002003269.

Lee, O. S. (1961), Observations of internal waves in shallow water, *Limnol. Oceanogr.*, *6*, 312–321, doi:10.4319/lo.1961.6.3.0312.

Moum, J. N., et al. (2007), Energy transport by nonlinear internal waves, *J. Phys. Oceanogr.*, *37*, 1968–1988, doi:10.1175/JPO3094.1.

Nash, J. D., and J. N. Moum (2005), River plumes as a source of large-amplitude internal waves in the coastal ocean, *Nature*, *437*(7057), 400–403, doi:10.1038/nature03936.

Pineda, J., et al. (2007), Larval transport and dispersal in the coastal ocean and consequences for population connectivity, *Oceanography*, *20*(3), 22–39.

Rosenfeld, L. K., et al. (1994), Bifurcated flow from an upwelling center: A cold water source for Monterey Bay, *Cont. Shelf Res.*, *14*, 931–964, doi:10.1016/0278-4343(94)90058-2.

Rosman, J. H., et al. (2008), Extracting Reynolds stresses from acoustic Doppler current profiler measurements in wave-dominated environments, *J. Atmos. Oceanic Technol.*, *25*(2), 286–306, doi:10.1175/2007JTECHO525.1.

Ryan, J. P., et al. (2005), Coastal ocean physics and red tides: An example from Monterey Bay, California, *Oceanography*, *18*(2), 246–255.

Ryan, J. P., et al. (2008), A coastal ocean extreme bloom incubator, *Geophys. Res. Lett.*, *35*, L12602, doi:10.1029/2008GL034081.

Scotti, A., and J. Pineda (2004), Observation of very large and steep internal waves of elevation near the Massachusetts coast, *Geophys. Res. Lett.*, *31*, L22307, doi:10.1029/2004GL021052.

Stashchuk, N., and V. Vlasenko (2009), Generation of internal waves by a supercritical stratified plume, *J. Geophys. Res.*, *114*, C01004, doi:10.1029/2008JC004851.

Thomas, L., and R. Ferrari (2008), Friction, frontogenesis, and the stratification of the surface mixed layer, *J. Phys. Oceanogr.*, *38*, 2501–2518, doi:10.1175/2008JPO3797.1.

Trask, R. P., and M. B. Briscoe (1983), Detection of Massachusetts Bay internal waves by synthetic aperture radar (SAR) on SEASAT, *J. Geophys. Res.*, *88*, 1789–1799, doi:10.1029/JC088iC03p01789.

Woodson, C. B., et al. (2009), Northern Monterey Bay upwelling shadow front: Observations of a coastally and surface-trapped buoyant plume, *J. Geophys. Res.*, *114*, C12013, doi:10.1029/2009JC005623.

Xing, J., and A. M. Davies (2005), Nonlinear interaction between wind-forced currents and near-inertial oscillations and internal waves in nearshore frontal regions, *J. Geophys. Res.*, *110*, C05003, doi:10.1029/2004JC002579.

J. A. Barth, College of Oceanic and Atmospheric Science, Oregon State University, 104 COAS Admin Bldg., Corvallis, OR 97331-5503, USA.

K. N. Carden, M. C. Lynch, and S. J. Teck, Department of Ecology, Evolution, and Marine Biology, University of California, Santa Barbara, CA 93106, USA.
B. S. Cheng, L. E. Garske, and M. J. Robart, Bodega Marine Laboratory, University of California, Davis, Bodega Bay, CA 94923, USA.
O. M. Cheriton, Ecology and Evolutionary Biology, University of California, Santa Cruz, CA 95064, USA.
T. C. Gouhier and A. Iles, Department of Zoology, Oregon State University, Corvallis, OR 97331, USA.
A. J. Haupt, K. T. Honey, M. L. Pinksy, and J. S. Stewart, Hopkins Marine Station, Stanford University, Pacific Grove, CA 93950, USA.
M. F. Hubbard, CODAR Ocean Sensors Ltd., 1914 Plymouth St., Mountain View, CA 94043, USA.
B. Mahoney, Department of Ecology, Evolution, and Marine Biology, University of California, Santa Cruz, CA 95060, USA.
M. A. McManus, Department of Oceanography, University of Hawai'i at Mānoa, 1000 Pope Rd., Honolulu, HI 96822, USA.
J. P. Ryan, Monterey Bay Aquarium Research Institute, PO Box 628, 7700 Sandholdt Rd., Moss Landing, CA 95039-9644, USA.
A. True, Civil and Environmental Engineering, Georgia Institute of Technology, Atlanta, GA 30332, USA.
L. Washburn, Geography Department, University of California, Santa Barbara, CA 93106, USA.
C. B. Woodson, Environmental Fluid Mechanics Laboratory, Stanford University, 473 Via Ortega, Stanford, CA 94305, USA. (bwoodson@stanford.edu)